Controlling Nanopore Size and Shape by Fluorosurfactant Templating of Silica

Bing Tan,[†] Hans-Joachim Lehmler,[‡] Sandhya M. Vyas,[‡] Barbara L. Knutson,[†] and Stephen E. Rankin*,[†]

Chemical and Materials Engineering Department, University of Kentucky, 177 Anderson Hall, Lexington, Kentucky 40506-0046, and Department of Occupational and Environmental Health, University of Iowa, 100 Oakdale Campus #124 IREH, Iowa City, Iowa 52242-5000

Received June 24, 2004. Revised Manuscript Received September 30, 2004

Fluorinated surfactants are a special class of surfactants that assemble into aggregates and form novel intermediate mesophases more easily than hydrocarbon surfactants. Despite their unique properties, researchers have only recently begun to explore the use of these surfactants as templates for porous inorganic materials. Here, we report a comprehensive investigation of the use of cationic fluorinated surfactants as templates for ordered nanoporous silica. A homologous series of perfluoroalkylpyridinium chloride surfactants with tail lengths between 6 and 12 carbons is synthesized and characterized. Using these surfactants in aqueous solution, materials are synthesized with pore structures that, as the tail length of the surfactant increases, include uniform wormhole-like pores, ordered 2-D hexagonal pores, and mesh phase pores. The smallest pore diameter observed in this series (2.19 nm by the KJS method) is among the smallest observed for a porous ceramic made with a single chain cationic surfactant. To avoid initial immiscibility of the silica precursor, a series of materials is also prepared from aqueous ethanol using the same series of surfactants. The products in this series include spherical particles with wormhole-like pores, spherical particles with radially oriented close-packed cylindrical pores, flower-like particles with radially oriented slit pores, and holey sheets of silica. For materials prepared in both water and in aqueous ethanol we find, as has been observed for hydrocarbon templates, that the pore sizes increase as the tail length of the surfactant increases, as long as the pore architecture remains the same. Unlike materials prepared with hydrocarbon surfactants, the pore architecture rapidly evolves toward mesh-phase and bilayer structures as the chain length increases. These investigations show that cationic fluorinated surfactants have significant potential not only as templates for controlling the size of familiar pore structures such as close-packed cylinders but also for developing ceramic materials with novel pore architecture.

Introduction

Mesoporous ceramics have been under increasing investigation for the past decade as novel materials for applications such as catalysis, drug delivery, sensors, optical applications, and fuel cell membranes.[1−6] These materials can be synthesized by several methods, but one useful approach is based on sol−gel hydrolytic polycondensation of alkoxysilanes in the presence of surfactants near room temperature. In this method, the surfactants act as pore templates by coassembling with ceramic precursors due to Coulombic forces or hydrogen bonding prior to material formation.[7−9] Upon surfactant removal, pores are left behind that mimic the size and ordering of micelles in lyotropic liquid crystals. By using different templates and different reaction conditions (such as pH, temperature, and surfactant/silica molar ratio), researchers have successfully made materials with controlled pore sizes and pore structures.[10−13]

A wide variety of hydrogenated surfactants, acids, and block copolymers have been investigated as templates to make mesoporous ceramic materials.[14−18] Fluorinated sur-

* To whom correspondence should be addressed. E-mail: srankin@engr.uky.edu. Telephone: (859) 257-9799.
[†] University of Kentucky.
[‡] Department of Occupational and Environmental Health.

(1) Brunel, D. *Micropor. Mesopor. Mater.* **1999**, *27*, 329.
(2) Descalzo, A. B.; Jimenez, D.; Marcos, M. D.; Martínez-Máñez, R.; Soto, J.; El Haskouri, J.; Guillém, C.; Beltrán, D.; Amorós, P.; Borrachero, M. V. *Adv. Mater.* **2002**, *14*, 966.
(3) Hayward, R. C.; Alberius-Henning, P.; Chmelka, B. F.; Stucky, G. D. *Micropor. Mesopor. Mater.* **2001**, *44*, 619.
(4) Wirnsberger, G.; Yang, P.; Scott, B. J.; Chmelka, B. F.; Stucky, G. D. *Spectrochim. Acta A* **2001**, *57*, 2049.
(5) Mal, N. K.; Fujiwara, M.; Tanaka, Y.; Taguchi, T.; Matsukata, M. *Chem. Mater.* **2003**, *15*, 3385.
(6) Halla, J. D.; Mamak, M.; Williams, D. E.; Ozin, G. A. *Adv. Funct. Mater.* **2003**, *13*, 133.
(7) Monnier, A.; Schüth, F.; Huo, Q.; Kumar, D.; Margolese, D.; Maxwell, R. S.; Stucky, G. D.; Krishnamurty, M.; Petroff, P.; Firouzi, A.; Janicke, M.; Chmelka, B. F. *Science* **1993**, *261*, 1299.
(8) Huo, Q. S.; Margolese, D. I.; Ciesla, U.; Feng, P. Y.; Gier, T. E.; Sieger, P.; Leon, R.; Petroff, P. M.; Schüth, F.; Stucky, G. D. *Nature* **1994**, *368*, 317.
(9) Tanev, P. T.; Pinnavaia, T. J. *Chem. Mater.* **1996**, *8*, 2068.
(10) Ciesla, U.; Schüth, F. *Curr. Opin. Colloid Interface Sci.* **1999**, *27*, 131.
(11) Ying, J. Y.; Mehnert, C. P.; Wong, M. S. *Angew. Chem., Int. Ed.* **1999**, *38*, 56.
(12) Selvam, P.; Bhatia, S. K.; Sonwane, C. G. *Ind. Eng. Chem. Res.* **2001**, *40*, 3237.
(13) Øye, G.; Sjöblom, J.; Stöcker, M. *Adv. Coll. Interface Sci.* **2001**, *89*−*90*, 439.
(14) Beck, J. S.; Vartuli, J. C.; Kenedy, G. J.; Roth, W. J.; Leonowicz, M. E.; Kresge, C. T.; Schmitt, K. D.; Chu, C. T.-W.; Olson, D. H.; Sheppard, E. W.; McCullen, S. B.; Higgins, J. B.; Schlenker, J. L. *J. Am. Chem. Soc.* **1992**, *114*, 10834.
(15) Huo, Q.; Margolese, D. I.; Stucky, G. D. *Chem. Mater.* **1996**, *8*, 1147.

10.1021/cm048991t CCC: $30.25 © 2005 American Chemical Society
Published on Web 01/26/2005

factants are intriguing as pore templates because their self-assembly behavior differs significantly from hydrocarbon surfactants. Because of weak intermolecular interactions, the fluorocarbon chains in these surfactants are not only hydrophobic but also lipophobic. As a result, fluorinated surfactants self-assemble much more easily than analogous hydrocarbon surfactants.[19,20] They aggregate in water at a critical micelle concentration generally equal to that of an analogous hydrocarbon surfactant of 50% greater tail length.[21] Also, fluorinated surfactants interact selectively with low-surface tension solvents (e.g., pressurized CO_2 and fluorocarbons), which may be used to facilitate extraction, recovery, and recycling of the fluorinated surfactants. The large van der Waals radius of fluorine as compared to hydrogen also makes fluorocarbons stiffer. This results in surfactants that favor aggregates with low curvature (such as cylinders, disks, and bilayers) and novel intermediate mesophases including rectangular and mesh phases.[22]

Fluorinated surfactants have been used several times to form ordered mesophase composites through complexation with hydrocarbon polyelectrolytes, as recently reviewed by Thünemann.[23] However, it is only within the last year that the association of fluorinated surfactants with inorganic ceramic precursors for materials synthesis has been investigated. In the first study to employ a fluorinated surfactant for ceramic synthesis, it was mixed with a nonionic hydrocarbon surfactant.[24] The surfactant acted as a thermal stabilizer to allow synthesis to occur at high temperatures. However, the pore size was too large to have been controlled by the fluorocarbon chain length. It is unlikely that the surfactant itself acted as a pore template, and in fact, Han et al. hypothesized that fluorinated surfactants alone are not suitable pore templates.[24] This hypothesis was almost immediately disproved by several recent reports of the use of cationic and nonionic fluorinated surfactants as templates for mesoporous silica.[25−27]

One of the aims of this work is to investigate the feasibility of making materials with small pore sizes by using single-chain cationic fluorinated surfactants. An established method to control the mesopore size in templated mesoporous ceramics is by the choice of surfactant tail chain length.[15,28,29] Single-chain hydrocarbon cationic surfactants with chains as short as C_8H_{17} have been used to make materials with small pore sizes.[29−32] However, surfactants with tails this short do not assemble into ordered structures easily, and all of the materials made with this surfactant have disordered pore structures.[29−32] Single-chain cationic surfactants with shorter chains offer limited prospects to be used as templates for ordered mesoporous ceramics because they do not self-assemble readily.[33] To overcome this limitation, Ryoo et al. began using double-chain hydrocarbon cationic surfactants.[31] The double-chain surfactant with C_8H_{17} tails produced 2-D hexagonal close packed (HCP) pores with an average diameter of 2.39 nm, and even smaller double-chained surfactants could be used.[31] An alternative approach is to use fluorinated surfactants. These surfactants are well-known for their low cmc (critical micelle concentration) as compared to analogous hydrocarbon surfactants.[20,22] For example, the eight-carbon fluorinated pyridinium chloride ($C_6F_{13}C_2H_4$-NC_5H_5-Cl) has a cmc of 16.2 mmol/L, which is approximately equal to that of the C12 hydrocarbon pyridinium chloride surfactant (15.5 mmol/L).[34] The low cmc means that fluorinated surfactants self-assemble more easily in solution, which we hypothesize will translate into easy coassembly with ceramic precursors to make small-pore mesoporous materials.

The second aim of this work is to demonstrate the potential to make materials with novel pore structures by using fluorinated surfactants. Researchers have already shown that not only pore sizes but also pore structures can be controlled by the surfactant structure. Different surfactants coassemble with silicates to generate mesoporous silicas with pore structures mimicking common lyotropic mesophases.[15] Silica products with wormhole-like,[35] 2-D hexagonal,[14,17] *Ia*3*d* cubic,[36] rectangular,[37] tetragonal,[38] orthorhombic,[39] sponge,[40] lamellar,[41] and vesicle[42] pore structures have been made with hydrocarbon surfactants. The materials with orthorhombic and tetragonal pore structures have been synthesized in films, in which stress and shrinkage during drying may contribute to the formation of the structure.[38,39] Despite this variety of pore structure, there are still several liquid crystal phase structures that have not been replicated in mesoporous silica.[43] Fluorinated surfactants can help to expand the range

(16) Pang, J. B.; Qiu, K. Y.; Wei, Y. *J. Non-Cryst. Solids* **2001**, *283*, 101.
(17) Kresge, C. T.; Leonowicz, M. E.; Roth, W. J.; Vartuli, J. C.; Beck, J. S. *Nature* **1992**, *359*, 710.
(18) Grosso, D.; Balkenende, A. R.; Albouy, P. A.; Ayral, A.; Amenitsch, H.; Babonneau, F. *Chem. Mater.* **2001**, *13*, 1848.
(19) Asakawa, T.; Hisamatsu, H.; Miyagishi, S. *Langmuir* **1995**, *11*, 478.
(20) Hoffmann, H.; Wurtz, J. *J. Mol. Liq.* **1997**, *72*, 191.
(21) Shinoda, K.; Hato, M.; Hayashi, T. *J. Phys. Chem.* **1972**, *76*, 909.
(22) Krafft, M. P.; Riess, J. G. *Biochemie* **1998**, *80*, 489.
(23) Thünemann, A. F. *Prog. Polym. Sci.* **2002**, *27*, 1473.
(24) Han, Y.; Li, D.; Zhao, L.; Song, J.; Yang, X.; Li, N.; Di, Y.; Li, C.; Wu, S.; Xu, X.; Meng, X.; Lin, K.; Xiao, F.-S. *Angew. Chem., Int. Ed.* **2003**, *42*, 3633.
(25) Rankin, S. E.; Tan, B.; Lehmler, H.-J.; Knutson, B. L. *Mater. Res. Soc. Symp. Proc.* **2003**, *775*, 47.
(26) Blin, J. L.; Lesieur, P.; Stébé, M. J. *Langmuir* **2004**, *20*, 491.
(27) Tan, B.; Dozier, A.; Lehmler, H. J.; Knutson, B. L.; Rankin, S. E. *Langmuir* **2004**, *20*, 6981.
(28) Lin, H. P.; Cheng, S. F.; Mou, C. Y. *Micropor. Mater.* **1997**, *10*, 111.
(29) Wloch, J.; Rozwadowski, M.; Lezanska, M.; Erdmann, K. *Appl. Surf. Sci.* **2002**, *191*, 368.
(30) Sayari, A.; Kruk, M.; Jaroniec, M. *Catal. Lett.* **1997**, *49*, 147.
(31) Ryoo, R.; Park, I.-S.; Jun, S.; Lee, C. W.; Kruk, M.; Jaroniec, M. *J. Am. Chem. Soc.* **2001**, *123*, 1650.
(32) Choma, J.; Burakiewicz-Mortka, W.; Jaroniec, M. *Colloids Surf., A* **2002**, *203*, 97.
(33) Beck, J. S.; Vartuli, J. C.; Kennedy, G. J.; Kresge, C. T.; Roth, W. J.; Schramm, S. E. *Chem. Mater.* **1994**, *6*, 1816.
(34) Wang, K.; Karlsson, G.; Almgren, M.; Asakawa, T. *J. Phys. Chem. B* **1999**, *103*, 9237.
(35) Zhang, W.; Pauly, T. R.; Pinnavaia, T. J. *Chem. Mater.* **1997**, *9*, 2491.
(36) Kumar, D.; Schumacher, K.; von Hohenesche, C. D. F.; Grün, M.; Unger, K. K. *Colloids Surf., A* **2001**, *187−188*, 109.
(37) Zhao, D.; Huo, Q.; Feng, J.; Kim, J.; Han, Y.; Stucky, G. D. *Chem. Mater.* **1999**, *11*, 2668.
(38) Doshi, D. A.; Huesing, N. K.; Lu, M. C.; Fan, H. Y.; Lu, Y. F.; Simmons-Potter, K.; Potter, B. G.; Hurd, A. J.; Brinker, C. J. *Science* **2000**, *290*, 107.
(39) Besson, S.; Ricolleau, C.; Gacoin, T.; Jacquiod, C.; Boilot, J.-P. *Micropor. Mesopor. Mater.* **2003**, *60*, 43.
(40) Behrens, P.; Glaue, A.; Haggenmüller, C.; Schechner, G. *Solid State Ionics* **1997**, *101−103*, 255.
(41) Tanev, P. T.; Liang, Y.; Pinnavaia, T. J. *J. Am. Chem. Soc.* **1997**, *119*, 8616.
(42) Lind, A.; Spliethoff, B.; Lindén, M. *Chem. Mater.* **2003**, *15*, 813.
(43) Hyde, S. T.; Schröder, G. E. *Curr. Opin. Colloid Interface Sci.* **2003**, *8*, 5.

of structures available in templated mesoporous ceramics because they easily form novel phases. The ability of 1*H*,1*H*,2*H*,2*H*-perfluorodecylpyridinium chloride to form mesh phases leads to the synthesis of a material (UK-2) with a mesh phase.[27] The possibility to make novel pore structures with these surfactants has not yet been fully investigated, however.

With these two aims in mind, a comprehensive investigation on the use of cationic fluorinated surfactants as pore templates is reported here. The surfactants are members of a homologous series of perfluoroalkylpyridinium chlorides with straight and branched chains ($C_nF_{2n+1}CH_2CH_2NC_5H_5$·Cl where $n = 4$, 6, 8, and 10 and $(CF_3)_2C_nF_{2n-1}CH_2CH_2$-$NC_5H_5$·Cl where $n = 5$ and 7). Of this series, the self-assembly behavior of the F_6H_2 (where F_i is a perfluoroalkyl group with i carbons, and H_j is an alkylene spacer with j carbons attaching the fluoroalkyl group to the pyridinium headgroup), F_8H_2, and $F_{10}H_2$ straight-chain surfactants in aqueous solution was studied with cryo-transmission electron microscopy (c-TEM).[34] The F_6H_2 surfactant was found to form globular micelles near the cmc. Both globular micelles and threadlike micelles were observed for the F_8H_2 surfactant at concentrations just above the cmc.[34] The $F_{10}H_2$ surfactant was found to form bilayers at surprisingly low concentrations, which indicates that this surfactant should be prone to form lamellar phases or vesicles.[34] Small-angle X-ray diffraction (XRD) showed that at high concentration in aqueous solution, F_8H_2 favors intermediate phases with low curvature.[44] As the F_8H_2 concentration increases, lyotropic mesophases found included a 2-D HCP phase, a rectangular phase, a trigonal mesh phase, a random mesh phase, and a lamellar phase.[44] Together, these c-TEM and XRD studies show that the perfluoroalkylpyridinium chlorides exhibit a broader range of micelle shapes and mesophases as the tail length increases than is usually observed in hydrocarbon surfactants. As we will show, a related variation is found in the pore structures of templated ceramic materials.

Experimental Procedures

Materials. The fluorocarbon surfactants ($C_nF_{2n+1}CH_2CH_2NC_5H_5$·Cl, $n = 4$, 6, 8, and 10; $(CF_3)_2C_nF_{2n-1}CH_2CH_2NC_5H_5$·Cl, $n = 5$ and 7) were synthesized as described previously by alkylation of anhydrous pyridine with the appropriate 1*H*,1*H*,2*H*,2*H*-perfluoroalkyl iodide followed by anion exchange (see Supporting Information for details and characterization).[19] Tetraethoxysilane (TEOS, 99+%) was obtained from Gelest. Concentrated aqueous ammonia (29 wt % NH_3, Merck), deionized ultrafiltered water, concentrated aqueous HCl (Fisher Scientific), and anhydrous ethanol (Aaper Alcohol) were used for materials synthesis.

Syntheses. Samples were made in aqueous (heterogeneous) and ethanol−water (homogeneous) solutions based on previously reported procedures.[36,45] For the procedure in aqueous solution, surfactant, water, and concentrated ammonia were first mixed for 1 h before the slow addition of TEOS. The mole ratios after the addition of TEOS in the aqueous series were 0.166 surfactant/154 H_2O/2.46 NH_3/1 TEOS. The mixed solution was aged with mild stirring at room temperature for 24 h and was then filtered and dried in air for 2 days. Finally, the surfactant was extracted by the sample being washed twice with acidic ethanol (5 mL of concentrated HCl in 150 mL of ethanol) before characterization. The products are designated as UKA*x*-1, where *x* is equal to 6, 8, 9b, 10, 11b, or 12 depending on the total number of carbons in the alkyl chain. A *b* following the number of carbons indicates a branched surfactant.

The materials synthesis in the water/ethanol solution followed a similar procedure except that ethanol was added to the initial solution before the addition of TEOS, and the aging time before the initial filtering was only 2 h. Two series were prepared from aqueous ethanol. In the first (samples UKH*x*-1 where $x = 6$, 8, 9b, 10, 11b, or 12), the mole ratios after the addition of TEOS were 0.30 surfactant/143 H_2O/56.7 C_2H_5OH/9.8 NH_3/1.0 TEOS. In the second (samples UKH*x*-2 where $x = 10$ or 12), the ratios were 0.075 surfactant/82.7 H_2O/28.3 C_2H_5OH/9.8 NH_3/1.0 TEOS.

Characterization. X-ray diffraction (XRD) patterns were recorded on a Siemens 5000 diffractometer using 0.154098 nm CuK_α radiation. Diffraction data were recorded at 2θ values between 1.8 and 10° with a step size of 0.02° and a scanning speed of 0.03 deg/min. For samples UKA10-1, UKH10-2, UKH12-2, a 0.008 deg/min scanning speed was used to increase the signal-to-noise ratio. Transmission electron microscope (TEM) images were collected with a JEOL 2010F electron microscope operating at 200 kV. Samples were dispersed in an acetone solution and then deposited on lacey carbon grids. Nitrogen sorption measurements were performed on a Micromeritics Tristar 3000 system. All samples were degassed at 150 °C for 4 h under flowing nitrogen prior to measurement. α_s plots were used to estimate the average pore texture properties (surface areas and pore volumes) relative to a reference macroporous silica material (LiChrospher Si-1000 silica, $S_{BET} = 22.1$ m^2 g^{-1} for $\omega = 0.135$ nm^2 per molecule).[32] The BJH method[46] or the BJH method with a modified statistical film thickness equation (KJS method)[47] was used to calculate the pore size distributions from the adsorption branch of the isotherms. Samples were assumed to have cylindrical pore shapes unless a slit pore shape was indicated. In this case, a modified BJH method for slit pores was adopted to estimate the pore size distributions.

Results and Discussion

Materials were prepared by room-temperature alkoxysilane hydrolysis under two sets of conditions leading to precipitation of white or off-white powders. The first set was prepared in heterogeneous aqueous solutions in which liquid−liquid phase separation occurred initially because of the immiscibility of TEOS in water. In the other set of conditions, ethanol was added to avoid the initial phase separation typically observed for a heterogeneous solution. In this section, we present and discuss the results for each series of samples.

Samples Made in Heterogeneous Aqueous Solutions. XRD patterns of the UKA series are compared in Figure 1. The *d* spacing is indicated for each reflection. Powder XRD patterns are reported only for the extracted materials because the as-synthesized materials have low contrast due to the presence of fluorine.[25] Sample UKA6-1 has one strong reflection and a second weak reflection. This diffraction pattern is consistent with weakly ordered 2-D hexagonal

(44) Wang, K.; Orädd, G.; Almgren, M.; Asakawa, T.; Bergenstähl, B. *Langmuir* **2000**, *16*, 1042.
(45) Grün, M.; Unger, K. K.; Matsumoto, A.; Tsutsumi, K. *Micropor. Mesopor. Mater.* **1999**, *27*, 207.
(46) Barrett, E. P.; Joyner, L. G.; Halenda, P. P. *J. Am. Chem. Soc.* **1951**, *73*, 373.
(47) Kruk, M.; Jaroniec, A.; Sayari, A. *J. Phys. Chem. B* **1997**, *101*, 583.

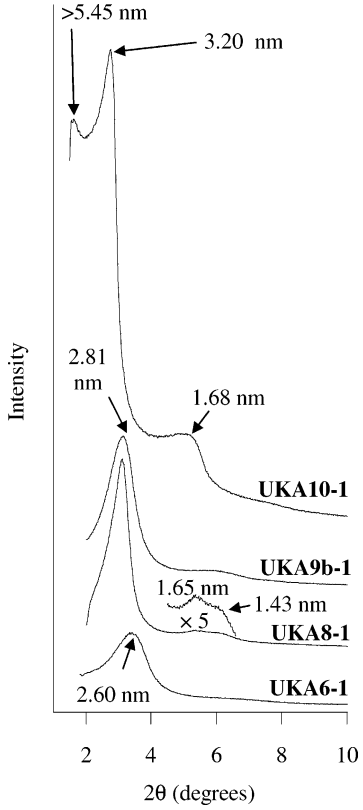

Figure 1. XRD patterns of samples UKA6-1, UKA8-1, UKA9b-1, and UKA10-1. Curves are offset vertically to make them more legible.

close packed pores or a disordered wormhole-like pore structure. The *d* spacing of the first reflection (2.60 nm) is among the smallest observed for silica powders made from single-chain cationic surfactants. Sample UKA8-1 has three distinct reflections, which are indexed to an ordered 2-D hexagonal structure.[25] Sample UKA9b-1 has two reflections that can be indexed to a lamellar or weakly ordered 2-D hexagonal/wormhole-like pore structure. The reflections of sample UKA10-1 are attributed to a random mesh phase structure, which is an intermediate phase found for the F_8H_2 surfactant in aqueous solution.[44] The TEM image confirms this assignment. The first reflection could not be clearly resolved for this sample, but in a comparable sample reported previously,[27] a similar reflection was indexed to pillars of silica that are uniformly but randomly spaced between continuous layers of silica. Because it is at the lower limit of the angles available on our instrument, we can only place a lower bound on the actual spacing between the pillars in this mesh-phase material equal to the highest *d* spacing that can be resolved, 5.4 nm. The second and third reflections are indexed to the (001) and (002) reflections of the mesh phase. The XRD patterns for samples UKA11b-1 and UKA12-1 (not shown) do not indicate any long-range structural order.

Representative TEM images of samples from this series are shown in Figure 2. UKA6-1 (Figure 2a) has a uniform wormhole-like pore structure. No evidence was found through TEM for hexagonal ordering in this sample. Sample UKA8-1 (Figure 2b) has an ordered 2-D hexagonal structure. Both hexagonal arrays of pores were observed, as seen in Figure 2b, as well as stripe patterns from viewing the edge

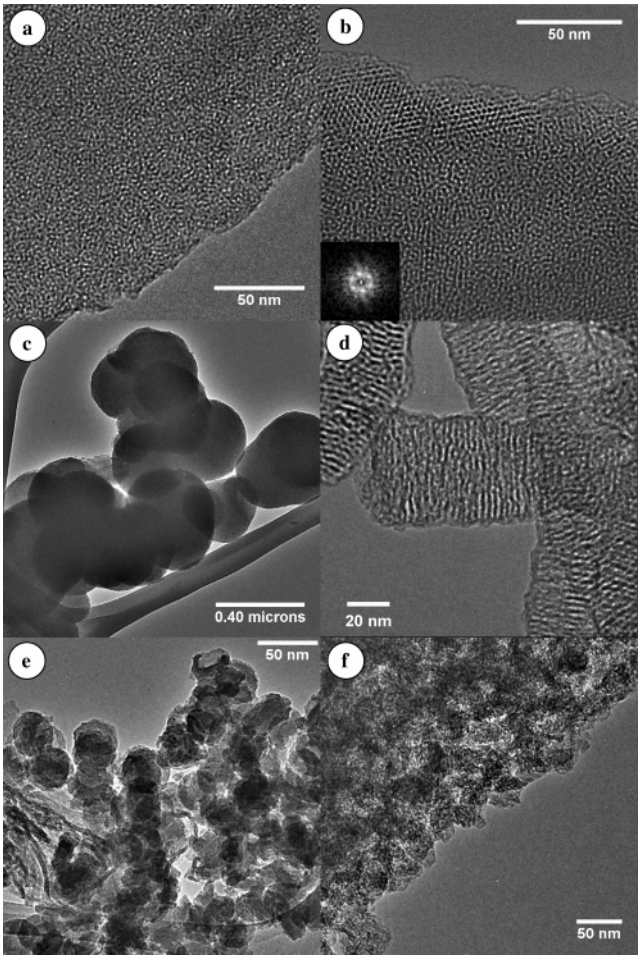

Figure 2. TEM images of samples (a) UKA6-1, (b) UKA8-1 with inset showing FFT of hexagonal region, (c) UKA9b-1, (d) UKA10-1, (e) UKA11b-1, and (f) UKA12-1.

of the (100) planes of pores. Figure 2b also shows some indication of disordered bicontinuous pores in the lower half of the image, but we found that regions that appear to be disordered sometimes reveal themselves to be ordered upon the sample being tilted. Both samples UKA6-1 and UKA8-1 have irregular particle morphology. Sample UKA9b-1 (Figure 2c) consists of spherical particles with wormhole-like pores within each particle. A low-resolution image is shown, to emphasize the smooth, spherical particle shape. Uniform spherical particles have been obtained by room-temperature synthesis of mesoporous silica in water/alcohol solution,[45,48] but this is an unusual morphology for particles synthesized in an alkaline aqueous solution, where more often particles are rough and irregular (sometimes faceted or elongated). A spherical particle shape implies that the surfactant−silica particles have sufficient time and driving force to reorganize at the interface and to minimize the surface area of contact between the particle and the surrounding fluid. This means either that the particles synthesized with UKA9b-1 remain fluid for a longer time than the samples prepared with other surfactants or that the surface tension at the surfactant−silica aggregate/solution interface is higher.

Sample UKA10-1 (Figure 2d) represents a departure from the previous three samples because it consists of elongated

(48) Grün, M.; Lauer, I.; Unger, K. K. *Adv. Mater.* **1997**, *9*, 254.

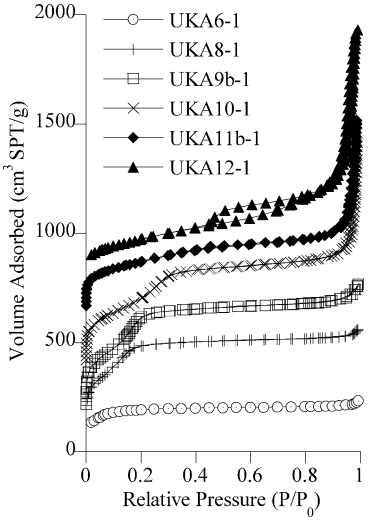

Figure 3. Nitrogen sorption isotherms for samples in the UKA series. Data are offset by 100, 200, 400, 650, and 800 cm^3 STP/g for UKA8-1, UKA9b-1, UKA10-1, UKA11b-1, and UKA12-1, respectively.

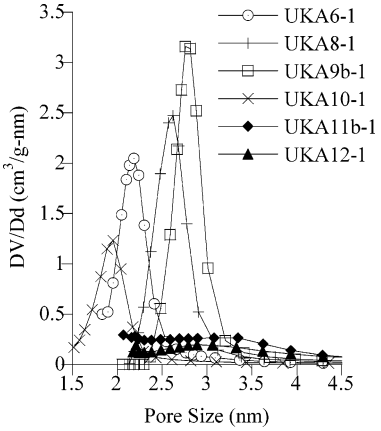

Figure 4. Pore size distributions for the UKA samples calculated using the KJS method.[47]

particles with a highly ordered layered pore structure oriented perpendicular to the main axis of the particles. The XRD pattern and TEM image for this sample are very similar to those of sample UK2, which was confirmed by extensive characterization by STEM to have a mesh phase structure, with silica micropillars holding apart continuous silica layers.[27]

UKA11b-1 and UKA12 both lack long-range order by XRD but have different short-range structures under TEM. Sample UKA11b-1 (Figure 2e) consists of round, almost spherical, nanoparticles. The TEM image shows no indication of pore ordering, but a few of the particles appear to be broken in the sample, and they may be hollow. There also are large flat sheetlike structures. Both of these structures are consistent with a distribution of single-walled vesicle-like aggregates in this sample. Sample UKA12-1 (Figure 2f) and appears to be composed of crumpled sheets of silica. This appearance could be caused by the collapse of a bilayer structure during extraction. Because of poor electron density contrast in the sample before extraction, it was not possible to confirm the formation of a lamellar phase before extraction. However, if $F_{10}H_2$ was to form bilayer structures (as the pure surfactant is known to do in water[34]), the heterogeneous density observed in TEM for UKA12-1 would be consistent with the collapse of such structures.

The isotherms and pore size distributions (PSD) of the UKA series are compared in Figures 3 and 4, respectively. Because UKA10-1 has a mesh-phase pore architecture, its PSD was calculated based on a slit pore shape. The isotherms of samples UKA6-1, UKA8-1, UKA9b-1, and UKA10-1 have sharp inflections, indicating capillary condensation in uniform pores. Consistent with this observation, these materials have narrow pore size distributions (Figure 4). Sample UKA10-1 has a significant amount of textural porosity, indicated by the upturn at high relative pressure. This textural porosity is present due to the voids within clusters of elongated particles that make up the sample (observed by low-resolution TEM but not shown). The pore size distributions for UKA11b-1 and UKA12-1 are very broad, and the pore volumes are low, which suggests that either an ordered silica−surfactant aggregate did not form or that it collapsed during extraction and drying. These two samples also have a large amount of textural porosity. This is consistent with the sample being composed of aggregates of rough particles with little internal porosity.

The pore properties of the UKA series are compared in Table 1. Because the KJS (modified BJH) method has been proven to be accurate for uniform cylindrical pores,[32] we take the pore width estimated by this method (w_{KJS}) as the best estimate of pore size for this series. We also report the BJH diameter[46] for comparison with existing mesoporous silica literature. Sample UKA6-1 has pores among the smallest (2.19 nm) reported by the KJS method for mesoporous silica prepared with a single-chain cationic surfactant. The pore width increases as the surfactant tail length increases at first (sample UKA8-1), but it decreases for sample UKA10-1. This is because both UKA6-1 and UKA8-1 have cylinder-based pore structures while UKA10-1 has slit pores; therefore, the pore width is calculated by a different formula. The BJH pore diameters in Table 1 increase monotonically across this series (except for UKA12-1, which has very little pore volume), but uniform cylindrical pores are assumed in this model. We know from TEM that the pores of UKA10-1 are slit-shaped.

The effect of branching is seen for sample UKA9b-1. Surfactants $(CF_3)_2C_5F_9CH_2CH_2NC_5H_5{\cdot}Cl$ and F_6H_2 have eight carbon atoms in the main chains. The difference in the chain length should be small. Sample UKA9b-1 (2.76 nm) has a slightly larger pore diameter than UKA8-1 (2.62 nm) but weaker ordering (Figure 1). The branching in the surfactant therefore appears to have expanded the core of the micelles but made micelles that more easily undergo fluctuations to create disordered, worm-like pores. Similarly, comparing samples UKA10-1 and UKA11b-1, the addition of one branching CF_3 group eliminates the long-range mesh phase ordering observed in sample UKA10-1. This leads to a sample with no discernible ordering by XRD or TEM and a relatively low pore volume. UKA11b-1 is more similar to sample UKA12-1 than to UKA10-1. For both UKA11b-1 and UKA12-1, the total surface area is almost the same as the external surface area, suggesting that these samples are composed primarily of macropores. The pore size distributions for both samples are very broad in the mesopore range,

Table 1. Pore Texture Parameters of the Samples Made in Aqueous Solution

sample	surfactant	d_1[a] (nm)	w_d[b] (nm)	w_{KJS}[c](nm)	w_{BJH}[d] (nm)	V_p[e] (cm^3/g)	S_t[f] (m^2/g)	S_{ex}[g] (m^2/g)
UKA6-1	$C_4F_9(CH_2)_2NC_5H_5$·Cl	2.60	2.20	2.19	0.9	0.43	884.2	23.7
UKA8-1	$C_6F_{13}(CH_2)_2NC_5H_5$·Cl	2.83	2.60	2.62	1.3	0.61	981.5	40.0
UKA9b-1	$(CF_3)_2C_5F_9(CH_2)_2NC_5H_5$·C l	2.81	2.62	2.76	1.4	0.66	943.0	76.2
UKA10-1[h]	$C_8F_{15}(CH_2)_2NC_5H_5$·Cl	3.20	1.80	1.95	1.8	0.58	850.7	150.5
UKA11b-1	$(CF_3)_2C_7F_{13}(CH_2)_2NC_5H_5$· Cl			3.34	2.0	0.08	590.2	348.8
UKA12-1	$C_{10}F_{21}(CH_2)_2NC_5H_5$·Cl			2.89	1.6	0.08	512.4	470.3

[a] d_1: d spacings of most prominent XRD reflections. For hexagonal structure, this is the (100) reflection, and for a mesh phase, it is the (001) reflection. [b] w_d: primary mesopores size calculated from $w_d = 1.213d_1(\rho V_p/(1+\rho V_p))^{1/2}$ for cylinder pore shapes and $w_d = d_1(\rho V_p/(1+\rho V_p))$ for slit pore shapes with $\rho = 2.2$ g cm^{-3}. [c] w_{KJS}: pore size at the maximum in the pore size distribution calculated with KJS modified BJH method.[30] For sample UKA10-1, the modified BJH method for slit pores was used.[27] [d] w_{BJH}: pore size at the maximum in the pore size distribution calculated with the BJH method. [e] V_p: primary mesopores volume from α_s plot. [f] S_t: total surface area from α_s plot. [g] S_{ex}: external particle surface area from α_s plot. [h] Calculations based on slit pore geometry assumption rather than cylindrical pores.

which confirms a lack of pore ordering in the extracted samples.

To summarize the observations of the heterogeneous samples made with the straight-chain surfactants (UKA series), as the surfactant chain length increases, the structure transforms in the sequence of wormhole-like, hexagonal, random mesh phase, and macroporous. The structural effect of the chain length of fluorinated surfactants on the pore structure is stronger than the effect of chain length of hydrogenated surfactants with similar chain lengths (C_nH_{2n+1}, $n = 8-18$).[29] While the pore diameter increases in a similar fashion as the alkyl chain length increases, the materials produced from hydrogenated cationic surfactants are most often wormhole-like or 2-D hexagonal cylindrical pores.[28,29] Contrasting this, the variety of pore structures in our materials mimics the sensitivity of micelle and mesophase structure to fluorocarbon tail length in perfluoroalkylpyridinium chloride surfactants. Cryo-TEM has shown that the micelle shape changes from spherical to worm-like to bilayers as the surfactant tail length increases in the F_6H_2 to $F_{10}H_2$ surfactant series.[34] Our own investigation of the F_6H_2 surfactant suggests that it forms 2-D hexagonal phases over a wide range of compositions at room temperature.[25] The F_8H_2 surfactant forms not only a 2-D hexagonal phase at low concentration but also intermediate phases including mesh phases over a large range of composition.[44] The pore structures that we see in the materials are consistent with a transition in the surfactant aggregate structure from cylindrical micelles (UKA6-1 and UKA8-1) to bilayer fragments or disk micelles (UKA10-1). The lack of order in UKA12-1 may be due to failure to coassemble or the collapse of a bilayer structure.

With the addition of the branching perfluoromethyl groups (CF_3) to the surfactants, the pore ordering is disrupted. We observe the structural transformations toward more disorder from UKA8-1 to UKA9b-1 and from UKA10-1 to UKA11b-1. The addition of a CF_3 group may reduce ordering either by preferentially swelling the micellar core or by preventing the fluorocarbons from organizing into a close-packed configuration within the micelle cores. For UKA9b-1, either effect may promote defects in a 2-D HCP cylindrical structure. For UKA11b-1, branching completely prevents ordering or may have led to bilayers that are unstable toward surfactant extraction.

Samples Made in Homogeneous Solution. TEOS and water are initially immiscible.[49] If TEOS is introduced to water without cosolvent or surfactant, the monomer will gradually dissolve as it is hydrolyzed and as ethanol is produced by hydrolysis. The initial immiscibility in an aqueous solution is more pronounced with fluorinated surfactant templates than with hydrogenated surfactants because the fluorinated chains do not emulsify the TEOS. To avoid the initial phase separation of the reactants, ethanol was added as a cosolvent for the UKH series. However, the presence of ethanol has been found to affect both the particle morphology and the pore structure of surfactant-templated silica.[50] The addition of ethanol helps to form monodisperse spherical particles both in the presence and in the absence of cationic surfactants.[48,51] At the same time, the presence of large amounts of ethanol would be expected to decrease the ordering of hydrocarbon aggregates by acting as a cosolvent to the surfactant tails.[52,53] Our experience with ethanol has been that it helps to dissolve solid perfluoroalkylpyridinium halide surfactants but that it is not as disruptive to mesophase formation as it has been found to be for hydrocarbon surfactants such as CTAB.[53]

With a large amount of ethanol, researchers have found that spherical particles with radially oriented cylindrical pores are produced from CTAB/silica mixtures at room temperature.[50] These particles were hypothesized to have MCM-48 (*Ia3d* cubic) cores. It was suggested that the MCM-48 cores form early in the synthesis process and act as seeds to generate a radial structure by growth of hexagonally patterned silica/surfactant aggregates from the facets of the seeds.[54] With this background in mind, we first determined whether spherical particles are produced under our synthesis conditions for cetyltrimethylammonium bromide (CTAB) and how the pores are oriented in those particles. A material was produced with the same mole ratios as the UKHx-1 series but with CTAB replacing the fluorinated surfactant. The 2-D hexagonal structure was found by XRD (not shown). The TEM image (Figure 5) confirms that under our conditions, CTAB templating leads to spherical particles, but this particle is one example of many in which the pores are oriented randomly rather than radially. Next, we will compare the

(49) Šefcík, J.; McCormick, A. V. *Catal. Today* **1997**, *35*, 205.
(50) Liu, S. Q.; Cool, P.; Collart, O.; Van der Voort, P.; Vansant, E. F.; Lebedev, O. I.; Van Tendeloo, G.; Jiang, M. H. *J. Phys. Chem. B* **2003**, *107*, 10405.
(51) Stöber, W.; Fink, A. *J. Colloid Interface Sci.* **1968**, *26*, 62.
(52) Huang, J.-B.; Mao, M.; Zhu, B.-Y. *Colloids Surf., A* **1999**, *155*, 339.
(53) Fontell, K.; Khan, A.; Lindstrom, B.; Maciejewska, D.; Puang-Ngern, S. *Colloid Polym. Sci.* **1991**, *269*, 727.
(54) Van Tendeloo, G.; Lebedev, O. I.; Collart, O.; Cool, P.; Vansant, E. F. *J. Phys. Cond. Matter* **2003**, *15*, S3037.

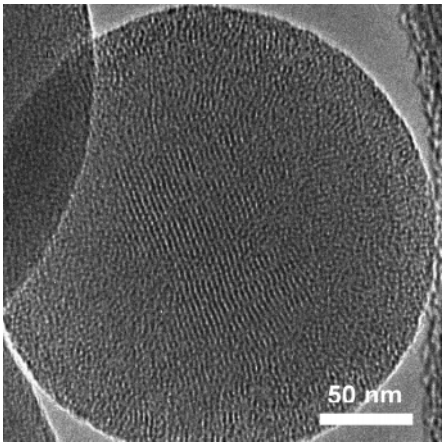

Figure 5. TEM image of the reference spherical MCM-41 sample prepared in aqueous ethanol.

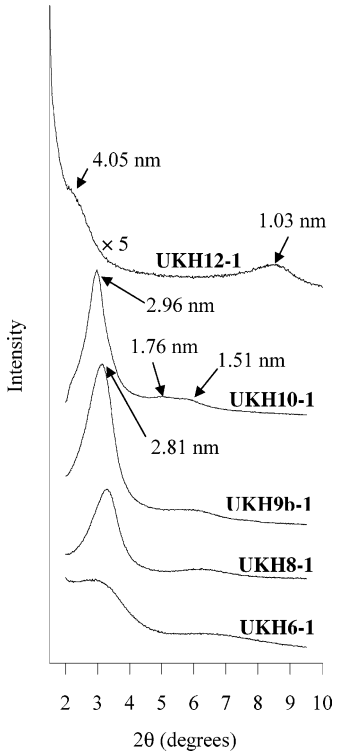

Figure 6. XRD patterns of samples UKH6-1, UKH8-1, UKH9b-1, UKH10-1, UKH11b-1, and UKH12-1. Curves are offset to make them more legible.

morphology and pore orientation of the fluorinated surfactant-templated materials to this product.

The XRD patterns for five of the UKH materials are shown in Figure 6. UKH6-1 has two broad reflections. The *d* spacing from the first reflection is (unexpectedly) larger than the first reflection for sample UKH8-1. This trend is similar to what was observed for the sample with double-chain hydrocarbon C6 surfactant, which also has an unexpectedly large *d* spacing.[31] The XRD patterns suggest that, similar to UKA6-1, samples UKH6-1, UKH8-1, and UKH9b-1 may have wormhole-like pore structures. This trend is inferred from the breadth of the XRD reflections for these samples and the lack of clearly resolved (110) and (200) reflections. The XRD pattern of UKH10-1, on the other hand, shows that it has a highly ordered 2-D hexagonal pore structure. No long-range ordering was found by XRD for UKH11b-1. The XRD pattern of UKH12- 1 has two reflections with a *d* spacing ratio of 1:1/4. This ratio can be interpreted as either a disordered lamellar structure (with reflections indexed as (001) and (004)) or as coming from a mixture of uniform pores of different sizes.

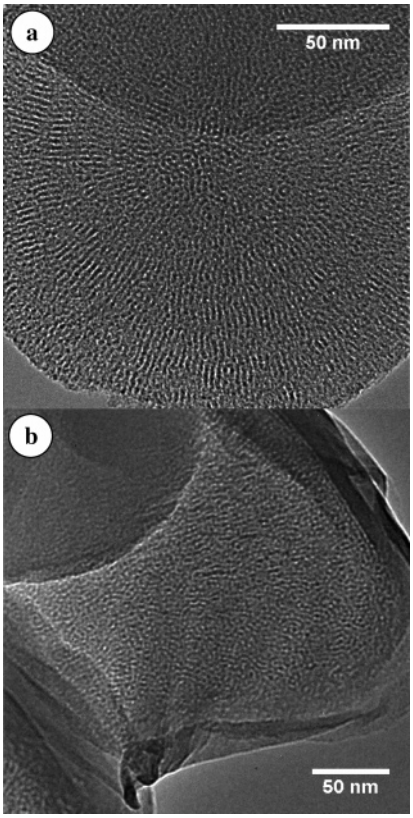

Figure 7. TEM images of the samples (a) UKH10-1 and (b) UKH12-1.

The TEM images of samples UKH6-1, UKH8-1, and UKH9b-1 (not shown) show that they have disordered wormhole-like pore structures, similar to that observed in sample UKA6-1, but all were found within spherical particles. On the other hand, sample UKH10-1 (Figure 7a) has well-ordered radially oriented pores within spherical particles. At the center of Figure 7a, one can see the 2-D hexagonal close packed cylindrical pores making up the radial structures in these particles. Both the XRD pattern and the TEM image show that this sample has the same structure as the spherical silica particle with radial pores prepared with a large amount of ethanol by van Tendeloo et al.[54] However, unlike the CTAB-templated samples,[54] UKH10-1 has a very small core region. We see no evidence for an *Ia*3*d* cubic core in the particles either, which is consistent with the absence of the gyroid phase from the phase diagram of the F_8C_2 surfactant.[44] The observation of good radial ordering of the pores of UKH10-1 brings into doubt the hypothesis that *Ia*3*d* cubic cores are responsible for radial pore formation in spherical silica particles. We propose instead that radial pores are formed by preferential orientation of the surfactant micelles normal to the particle interface. The promised "future study" was reviewed, accepted and published while the current manuscript was under consideration.[55]

(55) Tan, B.; Rankin, S. E. *J. Phys. Chem. B.* **2004**, *108*, 20122.

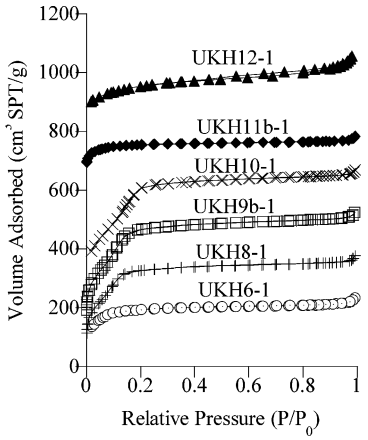

Figure 8. Nitrogen sorption isotherms for UKH series. Data are offset by 100, 200, 600, and 800 cm^3 STP/g for UKH9b-1, UKH10-1, UKH11b-1, and UKH12-1, respectively.

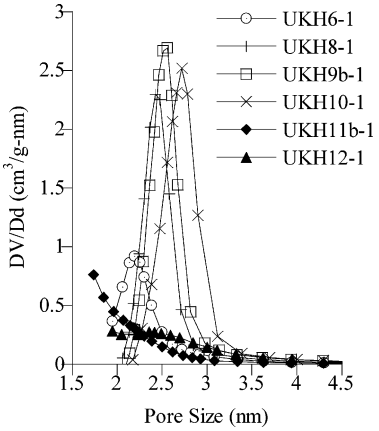

Figure 9. Pore size distributions for the UKH samples calculated using the KJS method.[47]

Sample UKH11b-1 (not shown) consists of spherical particles without any ordered pore structure. Sample UKH12-1 contains a mixture of irregular rough particles and spherical particles. Some of the particles appear to be organized as sheets of silica, as shown in Figure 7b. A mottled striped pattern with inter-stripe spacing of 3.0 nm is observed in the irregular particles, suggesting that the sheet that makes up this sample may contain cylindrical or disklike micelles. It is unusual to find irregular particles in materials synthesized under the high ethanol and ammonia conditions of the Stöber process. This process is an established method of forming perfectly spherical, uniform particles of silica which are either nonporous[51] (in ammonia solution) or mesoporous (with surfactant templates).[45,48,50,54] The reason may be that the micellar aggregates formed from the $F_{10}H_2$ surfactant are so rigid that they cannot be incorporated into spherical particles under these conditions.

The isotherms and pore size distributions of the UKH series of samples are shown in Figures 8 and 9. Most of the samples have large surface areas and narrow pore size distributions. The pore texture properties calculated by α_s-plot are shown in Table 2. UKH6-1 has the same pore diameter (2.19 nm) as UKA6-1. UKH8-1 (2.42 nm) has a smaller pore size than UKA8-1 (2.62 nm). Similar to UKA9b-1 and UKA8-1, UKH9b-1 (2.56 nm) has a larger pore size than UKH8-1. UKH10-1 has an ordered hexagonal structure, which is different than UKA10-1. Because the pore structure is similar in the series from UKA6-1 to UKA10-1, the pore size increases monotonically in this series.

Because significant internal pore volume is observed for sample UKH12-1, it seems that the templating process worked better than for UKA12-1. The inconsistency between the pore diameter calculated from the pore texture characteristics (w_d) and from the KJS method (w_{KJS}) of UKH12-1 may be because assumptions in the method of evaluating w_d. The former is calculated by assuming uniform cylindrical pores, for which $w_d = 1.213d_1(\rho V_p/(1 + \rho V_p))^{0.5}$ with $\rho = 2.2$ g/cm^3 for the density of amorphous SiO_2. We have found, for a series of F_6H_2 templated particles prepared with varying surfactant/Si ratio, that when the mesopores are not perfectly ordered, the pore width is underestimated by this equation. Another explanation for the unexpected small w_d value for sample UKH-12 is that it indicates that this sample may have a structure other than HCP. If it had a HCP structure similar to UKH10−1, the pore size of this sample should be larger since a template with a longer tail was used. Similar to the UKA heterogeneous series, as the fluorocarbon chain length increases in the UKH series, the pore structures transform from wormhole-like to hexagonal (with F_8H_2). However, a stable mesh phase structure is not observed, and instead for the F_9H_2 and $F_{10}H_2$ surfactants, no stable porous structure was obtained after extraction.

Second Series of Samples Made in Homogeneous Solutions. The samples UKA12-1 and UKH12-1, made with the $F_{10}H_2$ fluorinated surfactant as the template, did not show very good long-range ordering, even when ethanol was added to the synthesis solution. This suggests that cationic surfactants with fluorinated chains that are too long may be difficult to use as pore templates. The reason may be that the surfactant/silica ratio is too large and leads to lamellar composites. To explore this issue further, one more sample (UKH12-2) was made with this surfactant with a lower surfactant/silica ratio. For comparison, the F_8H_2 fluorinated surfactant was also used to make a sample, UKH10-2, under the same conditions. The mole ratios are given in the Experimental Procedures, and the synthesis procedure is the same as was described for the UKHx-1 series.

Table 2. Pore Texture Parameters of the Samples Made in Ethanol−Water Solution[a]

sample	surfactant	d_1 (nm)	w_d (nm)	w_{KJS} (nm)	w_{BJH} (nm)	V_p (cm^3/g)	S_t (m^2/g)	S_{ex} (m^2/g)
UKH6-1	$C_4F_9(CH_2)_2NC_5H_5{\cdot}Cl$	2.85	2.18	2.19	0.9	0.27	576.7	22.9
UKH8-1	$C_6F_{13}(CH_2)_2NC_5H_5{\cdot}Cl$	2.66	2.36	2.42	1.1	0.52	875.0	23.6
UKH9b-1	$(CF_3)_2C_5F_9(CH_2)_2NC_5H_5{\cdot}Cl$	2.81	2.56	2.56	1.2	0.59	897.0	28.1
UKH10-1	$C_8F_{15}(CH_2)_2NC_5H_5{\cdot}Cl$	2.96	2.76	2.72	1.5	0.66	977.1	25.4
UKH11b-1	$(CF_3)_2C_7F_{13}(CH_2)_2NC_5H_5{\cdot}Cl$					0.14	320.9	15.5
UKH12-1	$C_{10}F_{21}(CH_2)_2NC_5H_5{\cdot}Cl$	4.00	2.22	3.32	2.1	0.12	215.8	40.1

[a] All of the variables have the same meanings as in Table 1.

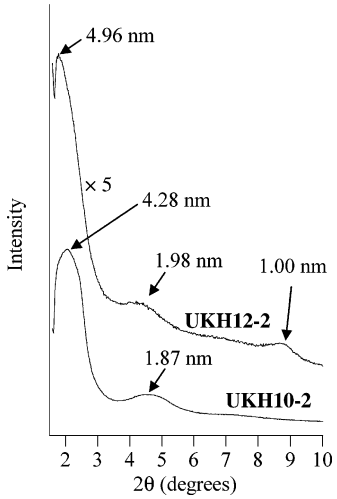

Figure 10. XRD patterns of samples UKH10-2 and UKH12-2.

The XRD pattern of UKH10-2 (Figure 10a) has two broad reflections, with a *d* spacing ratio of 2.1. While this ratio would ordinarily be indexed to a lamellar structure, particles with cylindrical, radially oriented mesopores have also been found to give broad, lamellar-like XRD patterns, due a lack of large aligned hexagonal domains. Compared to the TEM image of UKH10-1 (Figure 7a), the pores in UKH10-2 appear to be less ordered relative to each other, and so the XRD reflections are broader and less intense. The XRD pattern for sample UKH12-2 has three weak reflections. The higher-angle reflections can be indexed to (001) and (002) reflections of a lamellar structure, but the low-angle reflection cannot be indexed to this structure. This reflection may come from a minority of disordered pores or pillars of a mesh phase or may be an as-yet unexplained consequence of the radial structure observed in TEM. The relative intensities of these reflections are much lower than those for UKH10-2, which indicates that this sample has a less ordered structure.

The TEM images of the two samples are shown in Figure 11. Both of the samples are spherical particles with radially oriented pores. For the sample UKH10-2 (Figure 11a), ordered cylindrical radial pores are observed. An electron diffraction pattern indicating hexagonal ordering was found for this sample, similar to what was observed for sample UKH10-1. However, the ordering is less than in UKH10-1, causing broader and weaker diffraction peaks.

Sample UKH12-2 (Figure 11b) has radial pores even though they do not appear to be close-packed cylinders. Pores arranged in layers (not shown) are observed in broken fragments of this sample, which is consistent with the lamellar or mesh phase XRD interpretation. The pore arrangement can be understood by looking at the center of the TEM image of a representative particle (inset of Figure 11b), where we should be looking straight into the edge of the particle. While the other particles with ordered pores in the UKH series show close-packed circles indicating a 2-D hexagonal structure, thin linear pore segments are seen even near the very center of the particles of sample UKH12-2 (Figure 11b). Figure 11b also shows an image near the edge of the particles with higher transmission intensity and suggests that there are many layers of material near the edge of the particles, giving them a rough appearance. The

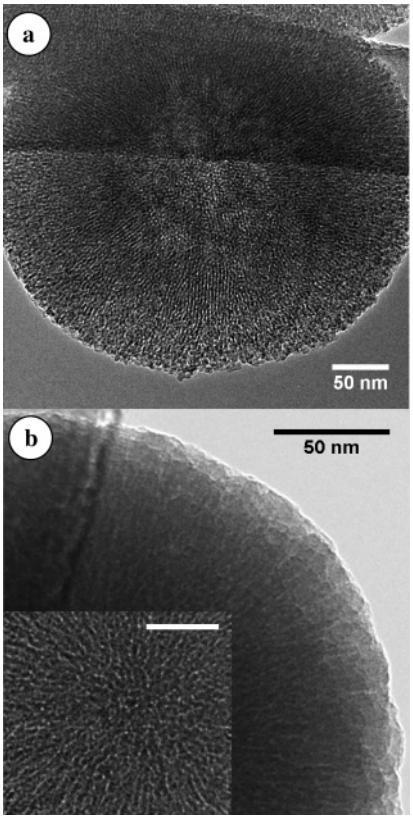

Figure 11. TEM image of the samples (a) UKH10-2 and (b) UKH12-2.

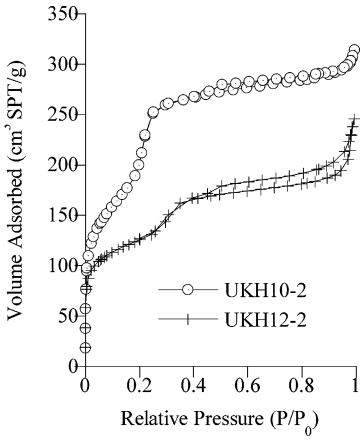

Figure 12. Isotherms of samples UKH10-2 and UKH12-2.

structure thus appears to be made up of silica layers arranged radially, somewhat like flower petals. This structure is consistent with the lamellar or mesh phase structure indicated by XRD.

The isotherms of and PSDs of the UKH10-2 and UKH12-2 samples are compared in Figures 12 and 13. Sample UKH10-2 has a larger surface area and bigger pore volume than UKH12-2. This is similar to the decrease in pore volume of mesh-phase sample UKA10-1 as compared to a close-packed cylindrical sample made from a smaller chain (UKA8-1). However, both samples UKH10-2 and UKH12-2 have type IV isotherms indicating that they have uniform mesopores, as indicated by the pore size distributions in Figure 13.

From this comparison and the results from the UKAx-1 and UKHx-1 series, we can draw the conclusion that even a

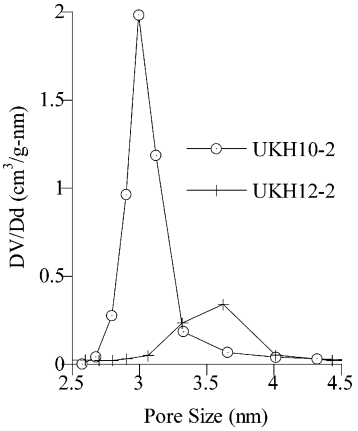

Figure 13. Pore size distributions of samples UKH10-2 and UKH12-2 calculated by the KJS method.[47]

surfactant such as $F_{10}H_2$ can be coaxed into forming an ordered porous silica particle structure, although it does so with difficulty. This may be the reason that fluorinated surfactants were disparaged as templates before.[24] Longer chains tend to promote bilayer and mesh phases, which can create materials with small pore volumes or which collapse upon surfactant extraction. In addition, the solubility of cationic fluorinated surfactants is more limited when the chains are too long. Despite the difficulty presented by the $F_{10}H_2$ surfactant, we were able to form ordered mesoporous structures using it and the F_6H_2 and F_8H_2 surfactants. The F_4H_2 and branched F_7H_2 and F_9H_2 surfactants could be used to precipitate silica particles with uniform, disordered mesopores.

Conclusion

A homologous series of cationic fluorinated surfactants has been used as templates to make silica powders with ordered mesopores. The smallest pore size (2.19 nm) of a material in this series was found in a sample with wormhole-like pores synthesized from the shortest surfactant (F_4H_2). The pore size of sample UKA6-1 was found to be as small or smaller than the pore sizes of wormhole-like particles formed from short-chain alkylammonium bromides.[32] As the tail length increased, larger pores were observed. However, there were inconsistencies in this trend as changes in the pore architecture occurred from wormhole-like to hexagonal to layered. This order of pore structure appearance was found as the chain length increased for both aqueous and ethanol/water synthesis solutions. The difference was the tail length at which the transitions occurred. For example, the F_8H_2 surfactant first formed a stable layered (mesh phase) structure in the aqueous samples, while only the $F_{10}H_2$ surfactant formed stable layered (radial) pores in aqueous ethanol. These results show greater sensitivity of pore structure to surfactant length for fluorinated surfactants than is observed in hydrocarbon surfactants. In addition, as was recently observed for hydrocarbon surfactants, particle synthesis in solutions with a large ethanol concentration leads to spherical, uniform particles with radially oriented pores, including an unusual radially oriented slit-shaped pore structure for sample UKH12-2.

Overall, we find that the unusual self-assembly properties of fluorinated surfactants carry over into pore templating. Because of facile self-assembly, the F_4H_2 surfactant produced particles with small, uniform pores. Because fluorinated surfactants prefer low-curvature aggregates and unusual intermediate phases, we were able to isolate both standard (wormhole-like, 2-D hexagonal) and novel (random mesh phase, radial slit) pore structures. The other advantage of these surfactants (the ability to interact selectively with low-surface tension solvents) will be explored in future contributions, as will be investigating methods for recycling these surfactants.

Acknowledgment. This material is based upon work partially supported by the National Science Foundation under Grant DMR-0210517. B.T. was supported by a Kentucky Research Challenge Trust Fund fellowship.

Supporting Information Available: Synthesis and characterization of the six fluorinated pyridinium surfactants ($C_nF_{2n+1}CH_2CH_2NC_5H_5{\cdot}Cl$ where $n = 4$, 6, 8, and 10 and $(CF_3)_2C_nF_{2n-1}CH_2CH_2NC_5H_5{\cdot}Cl$ where $n = 5$ and 7). This material is available free of charge via the Internet at http://pubs.acs.org.

CM048991T